Geochemical Perspectives Letters

Direct precipitation of siderite in ferruginous environments

A. Grengs[1,2], G. Ledesma[3,4], Y. Xiong[5], S. Katsev[6,7], S.W. Poulton[5], E.D. Swanner[4], C. Wittkop[2*]

OPEN ACCESS
https://doi.org/10.7185/geochemlet.2414

Abstract

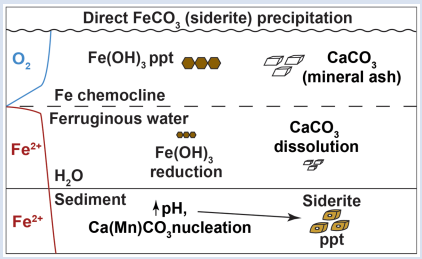

Siderite ($FeCO_3$) is often assumed to precipitate from dissimilatory reduction of Fe-(oxyhydr)oxides, but geochemical and mineralogical analyses from ferruginous (anoxic, Fe-rich) Canyon Lake, USA, suggest Fe-carbonate represents a direct early precipitate unrelated to substantial oxide burial. X-ray absorption near edge structure (XANES) spectroscopy of sediment trap materials and an anoxic sediment core indicated a mixture of Fe(II) and Fe(III) in water column particulates and ferruginous surface sediments, while all Mn phases were reduced. About 60 cm below the sediment–water interface, Fe-Mn carbonates were detected by X-ray diffraction and XANES, while Fe extended X-ray absorption fine structure (EXAFS) spectra were best fit with combinations of a biogenic Fe-oxyhydroxide ("Bio Fe"), greigite, and siderite. Sediment Fe speciation indicates a large pool of reduced Fe with a minor component of oxides. Although we found no evidence of significant carbonate phases above or below the 60 cm horizon, equilibrium modelling indicates siderite supersaturation throughout surface sediment porewater, with pH as the primary control on supersaturation. We conclude that delivery of wildfire ash to sediments increased pH, initiating siderite precipitation from ferruginous porewater.

Received 17 November 2023 | Accepted 22 April 2024 | Published 30 April 2024

Introduction

Siderite ($FeCO_3$) occurs in sediments throughout Earth's history (Ohmoto *et al.*, 2004) and is a common component in Precambrian iron formations (IFs; Konhauser *et al.*, 2017). Despite the diversity of environments in which siderite occurs, two mechanisms are generally considered to drive its formation: 1) direct precipitation from an anoxic and iron-enriched (ferruginous) fluid; and 2) as a diagenetic product derived from reduction of primary iron (oxyhydr)oxides coupled to microbial organic carbon remineralisation (Heimann *et al.*, 2010). While dissimilatory reduction of reactive iron (oxyhydr)oxides, such as ferrihydrite, may explain the negative C-isotopic composition and textures of many lacustrine siderite occurrences (Vuillemin *et al.*, 2019), the textures and C-isotope signatures of well-preserved Precambrian IFs are also consistent with precipitation from ferruginous seawater (Beukes *et al.*, 1990; Siahi *et al.*, 2020; Riding *et al.*, 2022), perhaps under a strong hydrothermal influence (Jiang and Tosca, 2019).

To constrain the conditions that govern natural siderite precipitation, we examined iron (Fe) and manganese (Mn) phases in water column particulates and recent sediments from ferruginous Canyon Lake (CL) in Michigan, USA. Modern ferruginous lakes serve as analogue systems, informing our understanding of biogeochemical dynamics in anoxic Precambrian oceans (Swanner *et al.*, 2020). Canyon Lake is an ideal site to investigate these processes, as its ferruginous bottom waters are poised near siderite supersaturation, and its water column has been chemically stable for at least the last 80 years (Lambrecht *et al.*, 2018). Found in a boreal shield setting, groundwater supplies the small CL basin with dissolved iron, and its water column chemistry and methane cycling embed processes similar to those thought to have dominated Precambrian oceans (Lambrecht *et al.*, 2020).

Methods

Multiparameter sondes were used to determine CL water column properties in 2018 and 2019, and water samples for cation and anion analysis were collected in May 2018, following standard procedures. A sediment freeze core was collected in February 2018, and sediment traps were deployed in 2019. Samples for iron speciation, XANES, and EXAFS were collected, processed under an N_2 atmosphere and stored anoxically until analysis. See Supplementary Information for Site Description, Methods, and full Results.

1. Earth Science Department, University of New Hampshire, 305 James Hall, Durham, NH 03824, USA
2. Department of Biochemistry, Chemistry, and Geology, Minnesota State University, Mankato, MN 56001, USA
3. Department of Earth Sciences, Memorial University of Newfoundland, St. John's, NL A1C 5S7, Canada
4. Department of Geological and Atmospheric Sciences, Iowa State University, Ames, IA 50011, USA
5. School of Earth and Environment, University of Leeds, Leeds, LS2 9JT, UK
6. Large Lakes Observatory, University of Minnesota Duluth, Duluth, MN 55812, USA
7. Department of Physics and Astronomy, University of Minnesota Duluth, Duluth, MN 55812, USA
* Corresponding author (email: chad.wittkop@mnsu.edu)

Results and Discussion

Iron and manganese phases in ferruginous waters. Centroid energies for Fe XANES pre-edge peaks from sediment trap material from 7.5, 15 and 20 m were ~7114 eV (Figs. 1, S-3), consistent with a mixture of Fe(II) and Fe(III). Best fits from linear combination fitting of Fe extended X-ray absorption fine structure (EXAFS) spectra for the sediment trap samples included, in order of contribution to fits, a biogenic Fe-oxyhydroxide ("Bio Fe"; Toner *et al.*, 2009), siderite, magnetite (Hansel *et al.*, 2005), green rust, and greigite. However, the quality of these fits was low, likely due to the limited amount of sample producing spectra with low signal to noise, or the presence of poorly crystalline phases. The main Mn K-edge peak energy in sediment trap samples (~6552 eV) was consistent with Mn(II) rather than Mn(III) or Mn(IV) (~6558 eV), indicating that Mn-oxides are not present in the water column (Fig. 1).

Sediment geochemistry and mineralogy. The sediments contain a large pool of highly reactive Fe (Fe_{HR}; average 3.59 ± 0.52 wt. %), with the Fe_{HR} pool dominated by unsulfidised Fe(II) phases ($Fe(II)_{unsulf}$), with a generally low concentration of poorly crystalline ferric (oxyhydr)oxide phases, such as ferrihydrite (Fe_{ox1}). The remaining Fe phases, comprising crystalline Fe (oxyhydr)oxides (Fe_{ox2}), magnetite (Fe_{mag}) and pyrite (Fe_{py}), were less significant throughout the core (Fig. 2; Table S-1).

Calculations using porewater dissolved inorganic carbon (DIC) and the solute chemistry of the deepest CL waters show siderite to be supersaturated throughout the porewater (Fig. 2). A sensitivity analysis adding additional dissolved Fe or DIC raised the saturation index only slightly; the most significant increase in siderite saturation scenarios came from increasing pH from 6.8 (the assumed porewater value) to 7.5 (Fig. 2), consistent with observations from ferruginous porewaters, where alkalinity increases due to organic carbon remineralisation (Vuillemin *et al.*, 2023).

Siderite was detected by XRD, with primary and secondary peaks observed at 31.62° and 52° 2θ (Fig. 3). A semi-quantitative ratio of siderite to quartz (I_{sid}/I_{qtz}) suggests siderite is concentrated mid-core (~60 cm), despite being supersaturated throughout the porewaters. SEM images from this interval detected <5 µm globular clumps with both dumbbell and spherical egg-shaped siderite morphologies that are consistent with growth in an organic matrix (Dupraz *et al.*, 2009); a few crystals also exhibited rhomb-like shapes. All observed crystal forms were consistent with siderite crystals grown in lab experiments (*e.g.*, Jiang and Tosca, 2019; Lin *et al.*, 2019) or observed in lacustrine settings (Wittkop *et al.*, 2014). Pre-edge peak fitting of sediment Fe XANES indicated predominantly Fe(II) (see Supplementary Information). Iron EXAFS of sediments were best fit by combinations of Bio Fe and siderite, with siderite having the greatest fit contribution (20.8 %) at 64 cm. Manganese XANES spectra were consistent with rhodochrosite ($MnCO_3$, which forms solid solutions with siderite) in samples from 64 and 110 cm.

Primary iron phases in Canyon Lake. Despite the highly reducing nature of the CL water column and sediments, some Fe_{ox1} persists in the sediment core. XANES spectra are consistent with the presence of mixed Fe(II)-Fe(III) phases (see Supplementary Information), perhaps green rust, which has been found in other ferruginous settings (Zegeye *et al.*, 2012). While authigenic magnetite has also been shown to be an early precipitate in ferruginous settings (Bauer *et al.*, 2020),

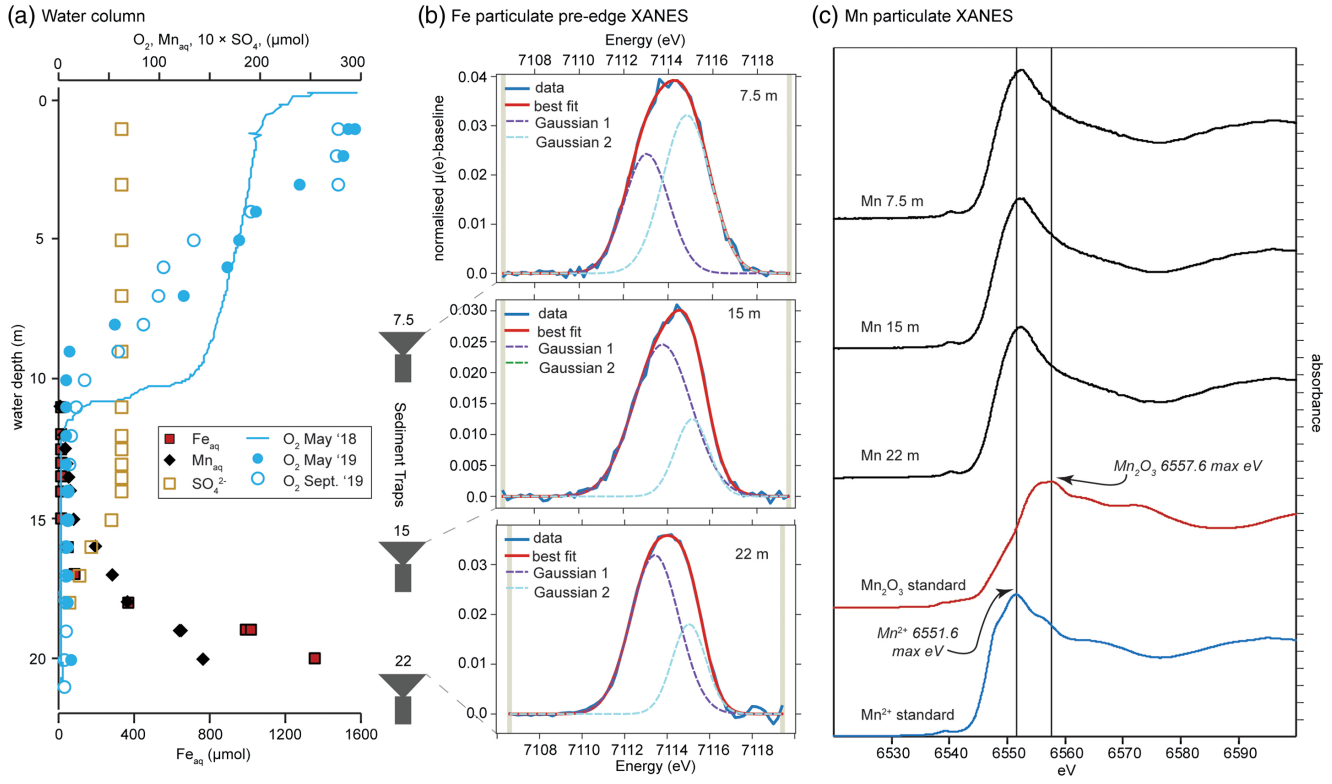

Figure 1 Geochemical and mineralogical characteristics of water column solutes and solid phases. **(a)** Dissolved solutes in the CL water column. The oxycline (decrease in dissolved oxygen) occurs between 7 and 12 m, and the chemocline (increase in dissolved Fe) occurs between 17 and 19 m. Sediment traps were deployed at 7.5, 15 and 22 m. **(b)** Sediment trap Fe XANES analyses. Pre-edge centroid energies are ~7114 eV, consistent with a mixture of Fe(II) and Fe(III). **(c)** Sediment trap Mn K-edge XANES analyses. Peaks have lower energy (~6552 eV) compared to Mn-oxides (~6558 eV), consistent with Mn(II) minerals.

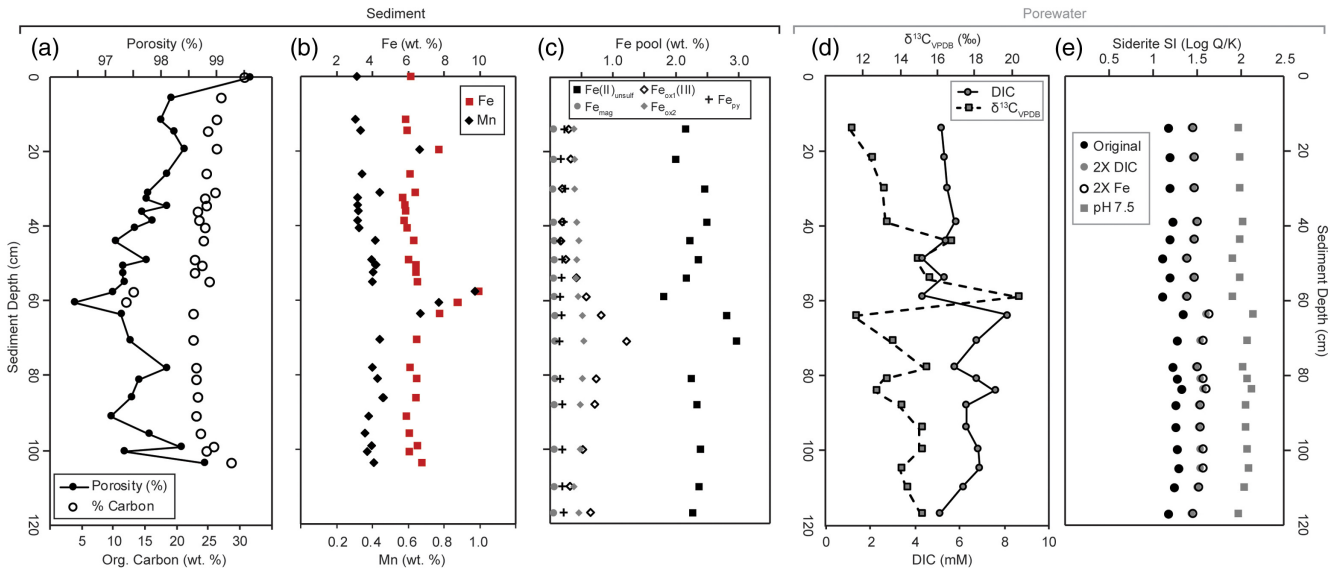

Figure 2 Bulk sediment and porewater geochemistry for the CL sediment core. **(a)** Porosity and organic carbon content of the sediments. The high organic carbon content of the sediments contributes to their high porosity. **(b)** Bulk sediment Fe and Mn content showing peaks at ~60 cm depth, which correspond to the presence of siderite (Fig. 3). **(c)** Iron speciation analysis demonstrating that much of the sediment Fe is contained in the $Fe(II)_{unsulf}$ pool. **(d)** Porewater dissolved inorganic carbon (DIC) concentration and isotope composition, showing a positive $\delta^{13}C$ signature consistent with the mass balance of depleted carbon lost to methane. **(e)** Siderite saturation index (SI), which assumes the Fe concentration (1.689 mmol/L) and pH (6.8) of deepest ferruginous water and measured porewater DIC values. Sensitivity scenarios were based on doubling DIC and Fe concentrations, and increasing pH to 7.5.

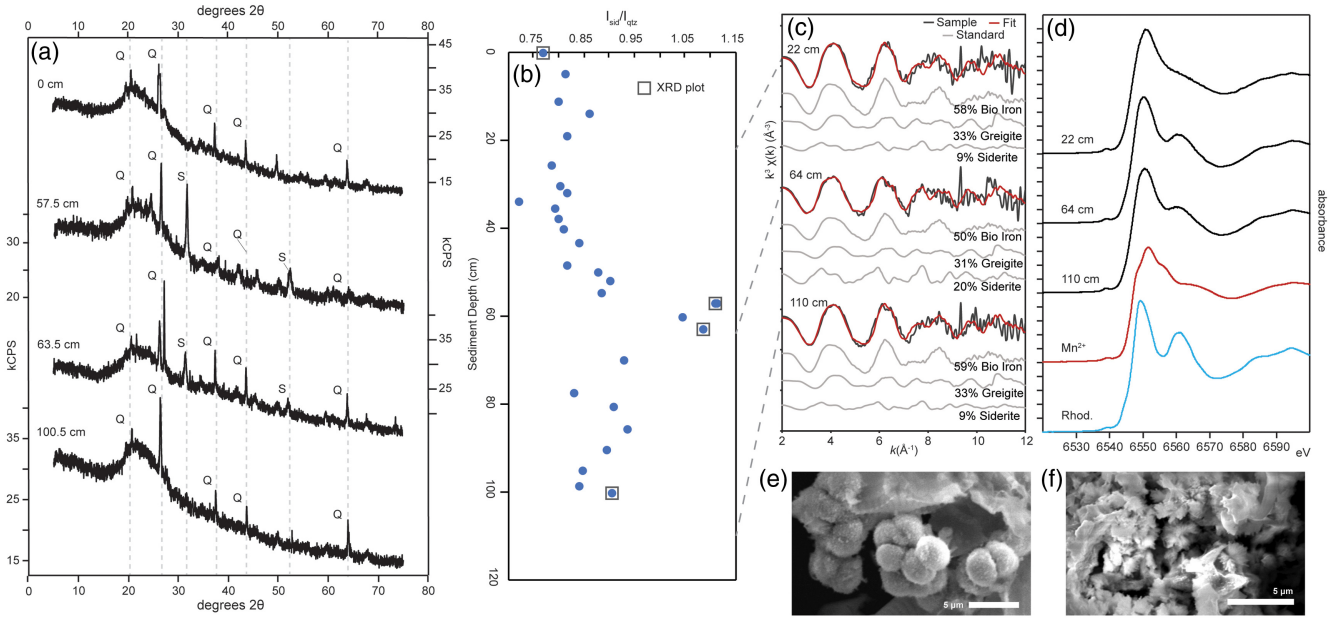

Figure 3 Sediment Fe phases. **(a)** Example XRD scans showing the emergence of siderite in mid-core depths (57.5 and 63.5 cm scans; Q = quartz peaks, S = siderite peaks). **(b)** Relative XRD intensity of the siderite peak normalised to the quartz peak (I_{sid}/I_{qtz}), showing an increase in siderite abundance mid-core. **(c)** Sediment Fe EXAFS spectra fit with linear contribution, showing values for Bio Fe, greigite, and siderite, with the greatest contribution (20 %) of siderite to fits in the 64 cm samples (Table S-5a). **(d)** Sediment Mn XANES dominated by reduced Mn(II), and the emergence of a distinctive double-peak of rhodochrosite in the 64 and 110 cm samples. **(e, f)** Example SEM images of twinned sphere and dumbbell crystal morphologies from the siderite-enriched interval, consistent with experimental precipitates of the mineral.

the concentrations in our extractions were very low (Fig. 2), and magnetite was not conclusively detected by EXAFS or XRD. Our EXAFS results suggest greigite is present in the sediments, but Fe extractions imply that this mixed-valence sulfide is a minor component of the Fe_{HR} pool (*i.e.* low concentrations of Fe sulfides), suggesting that the EXAFS analysis is highly sensitive to the presence of sulfides, or is perhaps interfered with by an unknown phase. Sulfide abundance is limited by the small sulfate reservoir in the water column available for reduction (Lambrecht *et al.*, 2018), though a contribution from an organic sulfur reservoir cannot be ruled out (*e.g.*, Phillips *et al.*, 2023).

The persistence of reduced Mn phases throughout the CL water column and sediments (Figs. 1 and 2) underscores the

limited ability of this system to oxidise the large reservoir of Fe and Mn from the ferruginous portion of the water column. The dominance of reduced Mn phases in sediment trap materials perhaps points to an external source of reduced solutes—in this case, groundwater input to the lake (Lambrecht *et al.*, 2018). Thus, Fe(III) delivery to CL sediments is limited, likely in the form of a poorly ordered Fe-(oxyhydr)oxide (Bio Fe), potentially supplemented by small quantities of greigite and/or green rust; a small component of Fe(III) may be added through detrital phases.

Controls on siderite occurrence. Although equilibrium modelling indicates siderite supersaturation throughout CL porewaters, carbonate minerals were only confirmed in one relatively restricted horizon, suggesting an inhibiting factor in the remaining intervals. The relatively slow kinetics of siderite precipitation, especially in the cold (~5 °C) bottom waters of CL, is a likely constraint; hence, a metastable precursor to siderite, such as green rust, may precipitate first. Carbonate green rust is closely associated with diagenetic siderite precipitation (Vuillemin *et al.*, 2019), and has been previously identified in the sediment traps from ferruginous Lake Matano (Zegeye *et al.*, 2012). Green rust ages to siderite in laboratory experiments (Halevy *et al.*, 2017), but the mechanisms which govern this transformation are not well understood (*e.g.*, Wiesli *et al.*, 2004), though pH is an important control on its behavior (*e.g.*, Guilbaud *et al.*, 2013). Although green rust potentially plays a role in the CL system, we were not able to conclusively identify it in this study.

The organic carbon-rich CL sediments also create an environment that inhibits carbonate precipitation. Over longer timescales, porewater alkalinity and pH are known to increase due to continued OM fermentation (Vuillemin *et al.*, 2023), but organic substrates may both inhibit and promote carbonate precipitation, dependent on the composition of functional groups, and the pH of the environment (Dupraz *et al.*, 2009). In CL sediments, intense fermentation (Lambrecht *et al.*, 2020) likely contributes to the inhibition of siderite precipitation by adding CO_2 to the pore fluids, buffering against significant increases in pH.

The appearance of crystalline siderite (XRD-detectable) ~60 cm below the ferruginous sediment–water interface suggests a precipitation barrier was overcome in this horizon, likely by an environmental change. While porewater diffusion smoothes the concentration profiles of solutes, diagenetic siderite precipitation may occur episodically due to environmental changes, such as lake level fluctuations (*e.g.*, Vuillemin *et al.*, 2023). However, CL has been stably stratified at least since the late 1930s (Lambrecht *et al.*, 2018), implying that climate-driven changes in lake mixing (*e.g.*, drought) were an unlikely influence in the interval where siderite occurs (see Supplementary Information). Wildfires are a more likely influence, as both historical accounts and tree ring records indicate that significant fires occurred in the forests surrounding CL as recently as the early 1900s (Muzika *et al.*, 2015). Calcium carbonate is a known product of wood combustion, and wildfire mineral ash is known to increase environmental pH in a variety of contexts (*e.g.*, Brito *et al.*, 2021).

Mineral ash deposition would stimulate an increase in porewater pH and deliver $CaCO_3$ to sediments. These changes would catalyse siderite precipitation by enhancing sorbtion of Fe and Mn ions to ash particles (Brito *et al.*, 2021), increasing the activity of CO_3^{2-} (Fig. 4), and providing nucleation sites for crystal growth, overcoming kinetic barriers to siderite precipitation (Jiang and Tosca, 2019; Lin *et al.*, 2019). The increase in abundance of bulk Fe and Mn in the siderite layer (Fig. 2) is consistent with a sorbtive process, and an ash layer may have resulted in reduced sediment porosity in the same interval, impeding porewater flow, leading to a localised increase in solute concentrations, further enhancing mineral precipitation potential. These observations suggest that the siderite layer in Canyon Lake sediments derives from a combination of depositional (ashfall, sorbtion) and diagenetic (post-depositional crystal growth) processes.

We cannot eliminate the possibility that another process, such as an overturn of lake stratification, drove enhanced Fe(III) delivery to CL sediments in the past, but it seems unlikely. Lake overturn would presumably be accompanied by oxidation of the CL's large isotopically light methane reservoir, which is inconsistent with our carbon isotope data. The association between mineral ashfall and sidertite precipitation we suggest is testable with high-resolution sediment chronology, advanced microscopy (*e.g.*, TEM), and/or charcoal analysis.

The pronounced influence of pH on siderite precipitation is linked to the dependence of siderite saturation on the concentration of the CO_3^{2-} ion (Fig. 4). Carbonate equilibrium dictates that $[CO_3^{2-}]$ scales linearly with total DIC but nonlinearly with $[H^+]$, due to the presence of a quadratic term (Supplementary Information). Hence, changing the pH by 1 unit has a stronger effect than a more substantial change in DIC. In CL porewaters where organic carbon remineralisation buffers H^+ fluctuations by increasing alkalinity (and consumption of H^+ by acetogens and methanogens), an external agent (*i.e.* mineral ash) is required to drive more substantial pH changes.

The detection of rhodochrosite by XANES in the same horizon where XRD indicates siderite illustrates the heterogeneous nature of carbonate precipitation in CL. Lacustrine siderites are commonly Mn-substituted (Swanner *et al.*, 2020), possibly linked to the more readily reducible nature of Mn-oxides relative to Fe-(oxyhydr)oxides (Vuillemin *et al.*, 2019). However, the lack of an Mn-oxide flux in CL suggests that a fundamental control on precipitation governs this occurrence of Mn-siderite, with competition from nucleation inhibitors (*e.g.*, Mg(II); Vuillemin *et al.*, 2019) or the differential solubilities of Ca-Mn-Fe carbonates (*e.g.*, Wittkop *et al.*, 2020) offering potential explanations. Thus, the occurrence of Mn-rich siderite in the geologic record (*e.g.*, Siahi *et al*, 2020; Swanner *et al.*, 2020) may be interpreted to reflect passive incorporation of dissolved Mn into the crystal structure, rather than reduction of Mn-oxides.

Biogeochemical Implications. Although siderite occurs in sediments throughout the geologic record, direct precipitation from Fe-enriched anoxic fluids is thought to be rare due to the slow kinetics of siderite precipitation (Jiang and Tosca, 2019). Modern process studies in oxygenated surface environments tend to encounter siderite only in early diagenetic settings (*e.g.*, Lin *et al.*, 2019). Hence it is often assumed that siderite precipitates following the deposition of an Fe-(oxyhydr)oxide precursor such as ferrihydrite, which is subsequently reduced in the sediments through microbial respiration, providing both dissolved Fe and the alkalinity needed to precipitate carbonate phases (Heimann *et al.*, 2010). However, our observations are not consistent with this traditional model, as the sediment Fe reservoir in CL is dominated by Fe(II) phases occurring below a persistently ferruginous water column.

While Fe-(oxyhydr)oxides are often invoked as precursors for Precambrian IF deposition (*e.g.*, Konhauser *et al.*, 2017), recent work has focused on the role of Fe-silicates in IF genesis (*e.g.*, Hinz *et al.*, 2021). In CL, direct precipitation of siderite below a ferruginous water column represents a significant Fe burial pathway that does not require precursor Fe-(oxyhydr)oxides or silicates. Hence, our work demonstrates that the presence of siderite in sediments should be carefully considered when interpreting past redox conditions, as direct precipitation pathways imply much lower oxygen levels at the sediment-water interface than diagenetic pathways involving Fe-(oxyhydr)oxide reduction.

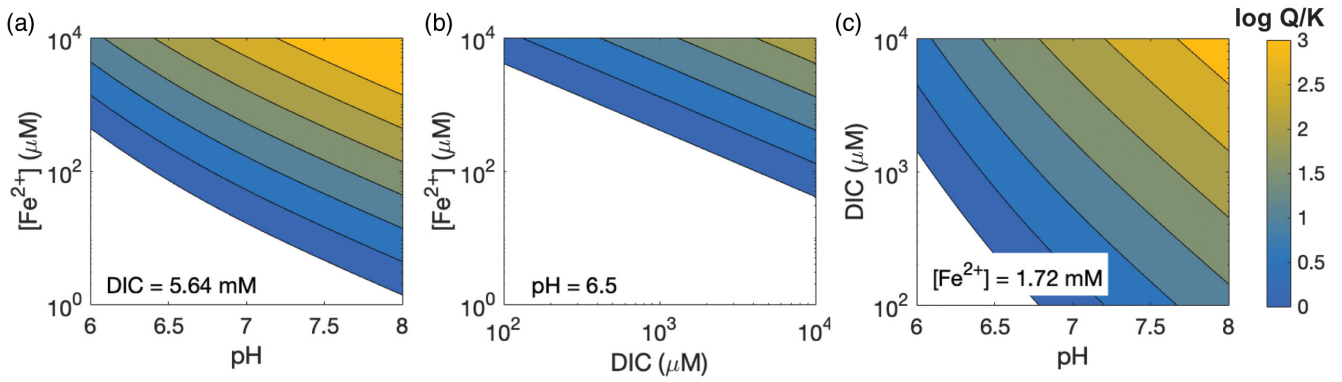

Figure 4 Relative influence of changes in porewater Fe concentration, pH and DIC on the saturation index of siderite. Inputs are based on water chemistry at 20 m, which is assumed to represent a minimum threshold for porewater concentrations. In general, iron concentrations above ~100 μM seem to be required for siderite precipitation, unless the pH is high.

Multiple studies highlight the importance of pH in governing both Fe-carbonate and Fe-silicate systems (Halevy *et al.*, 2017; Jiang and Tosca, 2019; Hinz *et al.*, 2021), as well as the evolution of stable phases from green rust precursors (Zegeye *et al.*, 2012). Could subtle variations in seawater silica concentration and pH have generated the silicate-carbonate banding observed in many Precambrian IFs (*e.g.*, James *et al.*, 1968; Beukes *et al.*, 1990)? A growing body of evidence supports this possibility, but additional experiments are needed to evaluate the role of pH changes and the presence of nucleation substrates in the direct precipitation of siderite (and associated Mn-carbonate).

In ancient seas, the role of wildfire ash in CL may have been played by processes that introduce calcium carbonate to more acidic ferruginous waters, including transgression over previously deposited carbonates, turbidites, or crystals settling from whiting events (*e.g.*, Morse *et al.*, 2003). The novel link between wildfire ash and enhanced siderite precipitation identified here may also imply a new pathway for enhancing carbon sequestration in methane-rich, ferruginous environments that appear to be widespread in boreal shield settings and postglacial lakes (Schiff *et al.*, 2017).

Acknowledgements

We thank Ben Harrison, Lance Hybben, Michael Mondry, and the Huron Mountain Club for field assistance. Jessica Heck, Kristina Brady Shannon, Ryan O'Grady and Amy Myrbo of the Continental Scientific Drilling Facility assisted with handling of the freeze core. Rose-Marie Muzika, Kerry Woods and Daniel Cziczo provided helpful discussion of fire history. This research utilized the Advanced Photon Source (APS), a U.S. Department of Energy (DOE) Office of Science User Facility operated for the DOE Office of Science by Argonne National Laboratory under Contract No. DE-AC02-06CH11357. Tianpin Wu and George Sterbinsky at 9BM assisted with data collection and analysis at the APS. Funding was provided by NSF-EAR 1660691, 1660761 and 1660873. Open access was supported by a Minnesota State University – Mankato Faculty Scholarship Grant.

Editor: Liane G. Benning

Additional Information

Supplementary Information accompanies this letter at https://www.geochemicalperspectivesletters.org/article2414.

Cite this letter as: Grengs, A., Ledesma, G., Xiong, Y., Katsev, S., Poulton, S.W., Swanner, E.D., Wittkop, C. (2024) Direct precipitation of siderite in ferruginous environments. *Geochem. Persp. Let.* 30, 1–6. https://doi.org/10.7185/geochemlet.2414

References

Bauer, K.W., Byrne, J.M., Kenward, P., Simister, R.L., Michiels, C.C., Friese, A., Vuillemin, A., Henny, C., Nomosatryo, S., Kallmeyer, J., Kappler, A., Smit, M.A., Francois, R., Crowe, S.A. (2020) Magnetite biomineralization in ferruginous waters and early Earth evolution. *Earth and Planetary Science Letters* 549, 116495. https://doi.org/10.1016/j.epsl.2020.116495

Beukes, N.J., Klein, C., Kaufman, A.J., Hayes, J.M. (1990) Carbonate petrography, kerogen distribution, and carbon and oxygen isotope variations in an Early Proterozoic transition from limestone to iron-formation deposition, Transvaal Supergroup, South Africa. *Economic Geology* 85, 663–690. https://doi.org/10.2113/gsecongeo.85.4.663

Brito, D.Q., Santos, L.H.G., Passos, C.J.S., Oliveira-Filho, E.C. (2021) Short-Term Effects of Wildfire Ash on Water Quality Parameters: A Laboratory Approach. *Bulletin of Environmental Contamination and Toxicology* 107, 500–505. https://doi.org/10.1007/s00128-021-03220-9

Dupraz, C., Reid, R.P., Braissant, O., Decho, A.W., Norman, R.S., Visscher, P.T. (2009) Processes of carbonate precipitation in modern microbial mats. *Earth-Science Reviews* 96, 141–162. https://doi.org/10.1016/j.earscirev.2008.10.005

Guilbaud, R., White, M.L., Poulton, S.W. (2013) Surface charge and growth of sulphate and carbonate green rust in aqueous media. *Geochimica et Cosmochimica Acta* 108, 141–153. https://doi.org/10.1016/j.gca.2013.01.017

Halevy, I., Alesker, M., Schuster, E.M., Popovitz-Biro, R., Feldman, Y. (2017) A key role for green rust in the Precambrian oceans and the genesis of iron formations. *Nature Geoscience* 10, 577–581. https://doi.org/10.1038/NGEO2978

Hansel, C.M., Benner, S.G., Fendorf, S. (2005) Competing Fe(II)-Induced Mineralization Pathways of Ferrihydrite. *Environmental Science & Technology* 39, 7147–7153. https://doi.org/10.1021/es050666z

Heimann, A., Johnson, C.M., Beard, B.L., Valley, J.W., Roden, E.E., Spicuzza, M.J., Beukes, N.J. (2010) Fe, C, and O isotope compositions of banded iron formation carbonates demonstrate a major role for dissimilatory iron

reduction in ~2.5 Ga marine environments. *Earth and Planetary Science Letters* 294, 8–18. https://doi.org/10.1016/j.epsl.2010.02.015

Hinz, I., Nims, C., Theuer, S., Templeton, A.S., Johnson, J.E. (2021) Ferric iron triggers greenalite formation in simulated Archean seawater. *Geology* 49, 905–910. https://doi.org/10.1130/G48495.1

James, H.J., Dutton, C.E., Pettijohn, F.J., Wier, K.L. (1968) *Geology and Ore Deposits of the Iron River-Crystal Falls District, Iron Country, Michigan*. USGS Professional Paper 570, United States Geological Survey, Washington, D.C. https://doi.org/10.3133/pp570

Jiang, C.Z., Tosca, N.J. (2019) Fe (II)-carbonate precipitation kinetics and the chemistry of anoxic ferruginous seawater. *Earth and Planetary Science Letters* 506, 231–242. https://doi.org/10.1016/j.epsl.2018.11.010

Konhauser, K.O., Planavsky, N.J., Hardisty, D.S., Robbins, L.J., Warchola, T.J., Haugaard, R., Lalonde, S.V., Partin, C.A., Oonk, P.B.H., Tsikos, H., Lyons, T.W., Bekker, A., Johnson, C.M. (2017) Iron Formations: A global record of Neoarchean to Paleoproterozoic environmental history. *Earth-Science Reviews* 172, 140–177. https://doi.org/10.1016/j.earscirev.2017.06.012

Lambrecht, N., Wittkop, C., Katsev, S., Fakhraee, M., Swanner, E.D. (2018) Geochemical Characterization of Two Ferruginous Meromictic Lakes in the Upper Midwest, USA. *Journal of Geophysical Research: Biogeosciences* 123, 3403–3422. http://dx.doi.org/10.1029/2018JG004587

Lambrecht, N., Katsev, S., Wittkop, C., Hall, S.J., Sheilk, C.S., Picarad, A., Fakhraee, M., Swanner, E.D. (2020) Biogeochemical and physical controls on methane fluxes from two ferruginous meromictic lakes. *Geobiology* 18, 54–69. https://doi.org/10.1111/gbi.12365

Lin, C.Y., Turchyn, A.V., Krylov, A., Antler, G. (2019) The microbially driven formation of siderite in salt marsh sediments. *Geobiology* 18, 207–224. https://doi.org/10.1111/gbi.12371

Morse, J.W., Gledhill, D.K., Millero, F.J. (2003) $CaCO_3$ precipitation kinetics in waters from the great Bahama bank: Implications for the relationship between bank hydrochemistry and whitings. *Geochimica et Cosmochimica Acta* 67, 2819–2826. https://doi.org/10.1016/S0016-7037(03)00103-0

Muzika, R.M., Guyette, R.P., Stambaugh, M.C., Marschall, J.M. (2015) Fire, Drought, and Humans in a Heterogeneous Lake Superior Landscape. *Journal of Sustainable Forestry* 34, 49–70. https://doi.org/1080/10549811.2014.973991

Ohmoto, H., Watanabe, Y., Kumazawa, K. (2004) Evidence from massive siderite beds for a CO_2-rich atmosphere before ~1.8 billion years ago. *Nature* 429, 395–399. https://doi.org/10.1038/nature02573

Phillips, A.A., Ulloa, I., Hyde, E., Agnich, J., Sharpnack, L., O'Malley, K.G., Webb, S.M., Schreiner, K.M., Sheik, C.S., Katsev, S., Raven, M.R. (2023) Organic sulfur from source to sink in low-sulfate Lake Superior. *Limnology and Oceanography* 68, 2716–2732. https://doi.org/10.1002/lno.12454

Riding, R., Liang, L., Fralick, P. (2022) Oxygen-induced chemocline precipitation between Archean Fe-rich and Fe-poor carbonate seas. *Precambrian Research* 383, 106902. https://doi.org/10.1016/j.precamres.2022.106902

Schiff, S.L., Tsuji, J.M., Wu, L., Venkiteswaran, J.J., Molot, L.A., Elgood, R.J., Paterson, M.J., Neufeld, J.D. (2017) Millions of boreal shield lakes can be used to probe Archean ocean biogeochemistry. *Scientific Reports* 7, 46708. https://doi.org/10.1038/srep46708

Siahi, M., Tsikos, H., Rafuza, S., Oonk, P.B.H., Mhlanga, X.R., van Niekerk, D., Mason, P.R.D., Harris, C. (2020) Insights into the processes and controls on the absolute abundance and distribution of manganese in Precambrian iron formations. *Precambrian Research* 350, 105878. https://doi.org/10.1016/j.precamres.2020.105878

Swanner, E.D., Lambrecht, N., Wittkop, C., Harding, C., Katsev, S., Torgeson, J., Poulton, S.W. (2020) The biogeochemistry of ferruginous lakes and past ferruginous oceans. *Earth-Science Reviews* 211, 1–43. https://doi.org/10.1016/j.earscirev.2020.103430

Toner, B.M., Santelli, C.M., Marcus, M.A., Wirth, R., Chan, C.S., McCollom, T., Bach, W., Edwards, K.J. (2009) Biogenic iron oxyhydroxide formation at mid-ocean ridge hydrothermal vents: Juan de Fuca Ridge. *Geochimica et Cosmochimica Acta* 73, 388–403. https://doi.org/10.1016/j.gca.2008.09.035

Vuillemin, A., Wirth, R., Kemnitz, H., Schleicher, A.M., Friese, A., Bauer, K.W., Simister, R., Nomosatryo, A., Ordonez, L., Ariztegui, D., Henny, C., Crowe, S.A., Benning, L.G., Kallmeyer, J., Russell, J.M., Bijaksana, S., Vogel, H., Towuti Drilling Project Science Team (2019) Formation of diagenetic siderite in modern ferruginous sediments. *Geology* 47, 540–544. https://doi.org/10.1130/G46100.1

Vuillemin, A., Mayr, C., Schuessler, J.A., Friese, A., Bauer, K.W., Lücke, A., Heuer, V.B., Glombitza, C., Henny, C., von Blanckenburg, F., Russell, J.M., Bijaksana, S., Vogel, H., Crowe, S.A., Kallmeyer, J. (2023) A one-million-year isotope record from siderites formed in modern ferruginous sediments. *GSA Bulletin* 135, 504–522. https://doi.org/10.1130/B36211.1

Wiesli, R.A., Beard, B.L., Johnson, C.M. (2004) Experimental determination of Fe isotope fractionation between aqueous Fe(II), siderite and "green rust" in abiotic systems. *Chemical Geology* 211, 343–362. https://doi.org/10.1016/j.chemgeo.2004.07.002

Wittkop, C., Teranes, J., Lubenow, B., Dean, W.E. (2014) Carbon- and oxygen-stable isotope signatures of methanogenesis, temperature, and water column stratification in Holocene siderite varves. *Chemical Geology* 389, 153–166. https://doi.org/10.1016/j.chemgeo.2014.09.016

Wittkop, C., Swanner, E., Grengs, A., Lambrecht, N., Fakrhaee, M., Myrbo, A., Bray, A., Poulton, S., Katsev, S. (2020) Evaluating a primary carbonate pathway for manganese enrichments in reducing environments. *Earth and Planetary Science Letters* 538, 116201. https://doi.org/10.1016/j.epsl.2020.116201

Zegeye, A., Bonneville, S., Benning, L.G., Sturm, A., Fowle, D.A., Jones, C., Canfield, D.E., Ruby, C., MacLean, L.C., Nomosatryo, S., Crowe, S.A., Poulton, S.W. (2012) Green rust formation controls nutrient availability in a ferruginous water column. *Geology* 40, 599–602. https://doi.org/10.1130/g32959.1